Article

Control of the Band-Edge Positions of Crystalline Si(111) by Surface Functionalization with 3,4,5-Trifluorophenylacetylenyl Moieties

Noah T. Plymale, Anshul A. Ramachandran, Allison Lim, Bruce S. Brunschwig, and Nathan S. Lewis

J. Phys. Chem. C, **Just Accepted Manuscript** • DOI: 10.1021/acs.jpcc.6b03824 • Publication Date (Web): 03 Jun 2016

Control of the Band-Edge Positions of Crystalline Si(111) by Surface Functionalization with 3,4,5-Trifluorophenylacetylenyl Moieties

Noah T. Plymale,[†] Anshul A. Ramachandran,[†] Allison Lim,[†] Bruce S. Brunschwig,[‡] and Nathan S. Lewis*[,†,‡,§]

[†]*Division of Chemistry and Chemical Engineering,* [‡]*Beckman Institute*, and [§]*Kavli Nanoscience Institute*, *California Institute of Technology, Pasadena, California 91125, United States*

ABSTRACT

Functionalization of semiconductor surfaces with organic moieties can change the charge distribution, surface dipole, and electric field at the interface. The modified electric field will shift the semiconductor band-edge positions relative to those of a contacting phase. Achieving chemical control over the energetics at semiconductor surfaces promises to provide a means of tuning the band-edge energetics to form optimized junctions with a desired material. Si(111) surfaces functionalized with 3,4,5-trifluorophenylacetylenyl (TFPA) groups were characterized by transmission infrared spectroscopy (TIRS), X-ray photoelectron spectroscopy (XPS), and surface recombination velocity (*S*) measurements. Mixed methyl/TFPA-terminated (MMTFPA) n- and p-type Si(111) surfaces were synthesized and characterized by electrochemical methods. Current density versus voltage and Mott-Schottky measurements of Si(111)–MMTFPA electrodes in contact with Hg indicated that the barrier height, Φ_b, was a function of the fractional monolayer coverage of TFPA (θ_{TFPA}) in the alkyl monolayer. Relative to Si(111)–CH_3 surfaces, Si(111)–MMTFPA samples with high θ_{TFPA} produced shifts in Φ_b of ≥0.6 V for n-Si/Hg contacts and ≥0.5 V for p-Si/Hg contacts. Consistently, the open-circuit potential (E_{oc}) of Si(111)–MMTFPA samples in contact with CH_3CN solutions that contained the 1-electron redox couples decamethylferrocenium/decamethylferrocene ($Cp^*_2Fe^{+/0}$) or methyl viologen ($MV^{2+/+\bullet}$)

shifted relative to Si(111)–CH_3 samples by +0.27 V for n-Si and by up to +0.10 V for p-Si. Residual surface recombination limited the E_{oc} of p-Si samples at high θ_{TFPA} despite the favorable shift in the band-edge positions induced by the surface modification process.

I. INTRODUCTION

The photovoltage produced by a semiconductor device is defined by the energetics of the junction.[1] Modern semiconductor devices rely heavily on p-n homojunctions to form a voltage-producing junction that is independent of the energetics of the interfacing phase, which can include metals,[2-3] metal oxides,[4-8] catalysts,[9-10] conductive polymers,[11-14] and electrolytes.[15-17] Many semiconductors cannot, however, be doped to form high-quality p-n homojunctions, and moreover the diffusive doping processes used to fabricate emitter layers is generally not compatible with small-grain-size polycrystalline thin-film semiconducting base layers.[18-19] In these cases it is often necessary to form a voltage-producing junction between the semiconductor and a contacting phase, e.g. a semiconductor liquid junction. Therefore, the development of methods to tune the semiconductor energetics relative to those of the contacting phase using thin or monolayer films could enable the use of new polycrystalline or thin-film materials in devices as well as lower the processing costs associated with device fabrication.

In the context of this work, the term "surface dipole" is used to refer to the unequal distributions of positive and negative charge at the silicon surface. This surface dipole produces an interfacial electric field that shifts the band-edge positions of the silicon relative to those in the contacting phase. Thus, shifts in band-edge positions produced by the surface dipole are reported in V or eV.

Control over the direction and magnitude of the surface dipole at the semiconductor surface, through chemical attachment of a molecular species, allows for manipulation of the

semiconductor's interfacial electric field to produce effective charge separation at the interface.[20] In principle, the barrier height, Φ_b, can be adjusted as a function of the surface dipole moment, allowing the relative band-edge positions to be tuned to drive a desired process (Figure 1). Control of the surface dipole for use in photoelectrochemical devices requires that the surface is stable under operational conditions and that a small or negligible fraction of the current is lost to surface recombination. A positive surface dipole has been produced on $GaInP_2$ and GaAs substrates by chemical functionalization.[21-23] The band-edge positions of Si(111) surfaces have also been modified to improve the energetics of junctions with metal oxides for use in catalytic applications.[24-25]

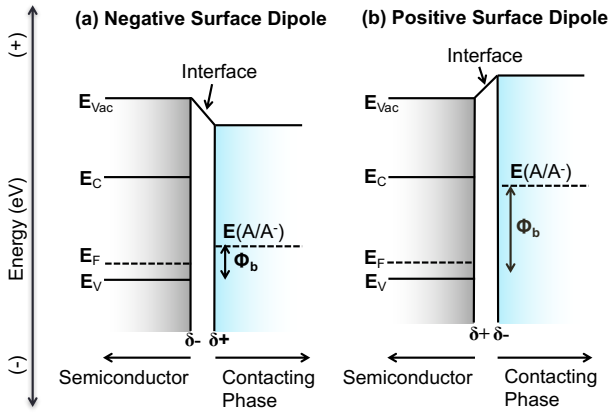

Figure 1. Effect of a surface dipole on the band-edge positions and barrier height, Φ_b, for a p-type semiconductor. The partial δ+ and δ– charges show the orientation of the dipole moment at the interface necessary to achieve the desired band-edge shift. The relative energy positions of the valence band, $\mathbf{E}_V$, the Fermi level, $\mathbf{E}_F$, the conduction band, $\mathbf{E}_C$, the vacuum level, $\mathbf{E}_{Vac}$, and the average electron energy of the contacting phase, $\mathbf{E}(A/A^-)$, are indicated.

Alkyl termination of Si surfaces using wet chemical methods could provide a scalable and versatile method to control the band-edge positions. A two-step halogenation/alkylation

process[26-31] has been shown to produce methyl-terminated Si(111) surfaces, Si(111)–CH_3, with low surface recombination velocities, *S*, that are stable for >500 h in air.[32-34] Relative to Si(111)–H surfaces, Si(111)–CH_3 surfaces are more stable against oxide formation[35-37] and are readily interfaced with metals without the formation of metal silicides.[38-39] However, methyl-termination of Si(111) produces a –0.4 V surface dipole,[38-42] which on p-Si surfaces will lower Φ_b at the Si interface and reduce the electric field at the junction that drives the charge separation.

Surface functionalization with groups that contain C–F bonds, such as 3,4,5-trifluorophenylacetylene (TFPA), should in principle produce a dipole moment opposite in sign to the C–H bonds in –CH_3 groups, and thus lead to a reversal of the negative dipole at p-type Si(111)–CH_3 surfaces. Mixed monolayer chemistry at Si(111) surfaces allows for functionalization of the surface with bulky groups that contain a desired functionality while maintaining low *S* and high Si–C termination.[7, 34, 43-45] A mixed methyl/TFPA (MMTFPA) surface could therefore provide desirable passivation of the Si surface while allowing for the dipole to be moved more positive as a function of fractional monolayer TFPA coverage, θ_{TFPA}. Additionally, the C–F bonds in the TFPA groups are chemically inert and oriented with a significant portion of the dipole moment normal to the surface. MMTFPA monolayers on Si(111) surfaces could provide a robust method for controlling the semiconductor band-edge positions to impart desirable interfacial energetics without requiring formation of a p-n homojunction. Accordingly, we describe herein the synthesis and characterization of Si(111)–MMTFPA surfaces, the electrochemical properties of these surfaces in contact with Hg, and the photoelectrochemical behavior of Si(111)–MMTFPA surfaces in contact with CH_3CN solutions that contain the 1-electron redox couples decamethylferrocenium/decamethylferrocene ($Cp^*_2Fe^{+/0}$) and methyl viologen ($MV^{2+/+\bullet}$).

II. EXPERIMENTAL

II.A. Materials and Methods. Water with a resistivity of ≥18.2 MΩ cm was obtained from a Barnstead E-Pure system. Ammonium fluoride (NH_4F(aq), 40%, semiconductor grade, Transene Co., Inc., Danvers, MA) was purged with Ar(g) (99.999%, Air Liquide) for ≥1 h prior to use. 3,4,5-trifluorophenylacetylene (TFPA, SynQuest Laboratories, Alachua, FL) was purified by four freeze-pump-thaw cycles, dried over activated 3 Å molecular sieves (Sigma Aldrich), and stored in a N_2(g)-purged glovebox (<10 ppm O_2(g)) in a foil-wrapped glass Schlenk tube. All other chemicals were used as received.

Si wafers were oriented to within 0.5° of the (111) crystal plane. Float-zone-grown Si wafers (University Wafer, Boston, MA) that were used for transmission infrared spectroscopy (TIRS) were double-side polished, not intentionally doped, had a resistivity of >2 kΩ cm, and were 525 ± 15 μm thick. Float-zone-grown Si wafers (FZwafers.com, Ridgefield Park, NJ) used for *S* measurements were double-side polished, not intentionally doped, had with a resistivity of 20–40 kΩ cm, and were 300 ± 25 μm thick. Czochralski-grown n-Si wafers (University Wafer, Boston, MA) used for electrochemical experiments were single-side polished, doped with phosphorus to a resistivity of 1.1–1.2 Ω cm, and were 380 μm thick. Czochralski-grown p-Si wafers (Silicon Quest International, San Jose, CA, or Addison Engineering, San Jose, CA) used for electrochemical experiments were single-side polished (Silicon Quest International) or double-side polished (Addison Engineering), doped with boron to a resistivity of 0.40–0.43 Ω cm, and were 300 ± 25 μm thick.

II.A.1. Preparation of lithium 3,4,5-trifluorophenylacetylide. In a 250 mL round-bottom flask that was connected to a Schlenk line, degassed and dried 3,4,5-trifluorophenylacetylene (TFPA, 1.95 g, 12.5 mmol) was dissolved in hexanes (100 mL, anhydrous, mixture of isomers,

≥99%, Sigma-Aldrich). The contents of the flask were cooled to –78 °C in a dry ice/acetone bath and were stirred vigorously while *n*-butyllithium (*n*-BuLi, 1.68 M in hexanes, 7.3 mL, 12.3 mmol, Sigma-Aldrich) was added dropwise via a syringe. The reaction was allowed to proceed at –78 °C for 30 min, after which the flask was allowed to warm to room temperature while being stirred for an additional 60 min, yielding a white slurry. The slurry was transferred under an inert atmosphere to an amber bottle, which was stored at 8 °C. Immediately before use, tetrahydrofuran (THF, anhydrous, ≥99.9%, Sigma-Aldrich) was added to the lithium 3,4,5-trifluorophenylacetylide (LiTFPA) slurry in 1:4 v/v THF:hexanes to solvate the product, forming a 0.10 M solution.

II.A.2. Preparation of Si(111)–H Surfaces. Wafers were cut to the desired size using a diamond-tipped scribe. The samples were washed sequentially with water, methanol (≥99.8%, BDH), acetone (≥99.5%, BDH), methanol, and water. The wafers were then immersed in a piranha solution (1:3 v/v of 30% H_2O_2(aq) (EMD): 18 M H_2SO_4 (EMD)) and heated to 95 ± 5 °C for 10–15 min. The solution was drained and the wafers were rinsed with copious amounts of water. The oxide was removed by immersing the wafers in aqueous buffered hydrofluoric acid (HF, semiconductor grade, Transene Co., Inc.) for 18 s, followed by a brief rinse with water. Atomically flat Si(111)–H surfaces were formed by anisotropic etching for 5.5 min in an Ar(g)-purged solution of NH_4F(aq).[33]. To remove bubbles that formed on the surface, the wafers were agitated at the start of every minute of etching, and the solution was purged throughout the etching process. After etching, the wafers were rinsed with water and dried under Ar(g).

II.A.3. Preparation of Si(111)–Cl Surfaces. The Si(111)–H wafers were transferred to a N_2(g)-purged glovebox with <10 ppm O_2(g) and rinsed with chlorobenzene (anhydrous, ≥99.8%, Sigma-Aldrich). The wafers were placed into a saturated solution of phosphorus pentachloride

(PCl_5, ≥99.998% metal basis, Alfa Aesar) in chlorobenzene, and were heated to 90 ± 2 °C for 45 min.[33] The addition of benzoyl peroxide, which has been used as a radical initiator,[46] was found not to be necessary to yield high-quality Si(111)–Cl surfaces. When the reaction finished, the wafers were removed from the reaction solution and rinsed sequentially with chlorobenzene and anhydrous THF.

II.A.4. Alkylation of Si(111)–Cl Surfaces. Si(111)–CH_3 surfaces were prepared by immersing the Si(111)–Cl surfaces in a 3.0 M solution of methylmagnesium chloride (CH_3MgCl, Acros Organics) and heating to 50 ± 2 °C for 12–24 h.[33]. Mixed methyl/TFPA (MMTFPA) monolayers (Scheme 1) were formed by first reacting Si(111)–Cl surfaces with LiTFPA (0.10 M in 1:4 v/v THF:hexanes) for 1–20 h at 23–65 °C in the absence of light. The wafers were then rinsed with THF and submerged in 3.0 M CH_3MgCl for 12–24 h at 50 °C.[7, 34, 43] Si(111)–TFPA surfaces were prepared by reacting Si(111)–Cl wafers with LiTFPA (0.10 M) at 65 °C for 10–20 h.

After completion of the reactions to yield the target surfaces, the wafers were removed from the reaction solution, rinsed with THF, and submerged in THF. The samples were removed from the glovebox and sonicated for 10 min in each of THF, methanol, and water. Following sonication, the wafers were rinsed with water and dried under Ar(g). For the fabrication of electrodes, wafers were broken into appropriately sized pieces, rinsed again with water, and dried under Ar(g).

Scheme 1. Synthesis of Si(111)–TFPA and Si(111)–MMTFPA Surfaces.

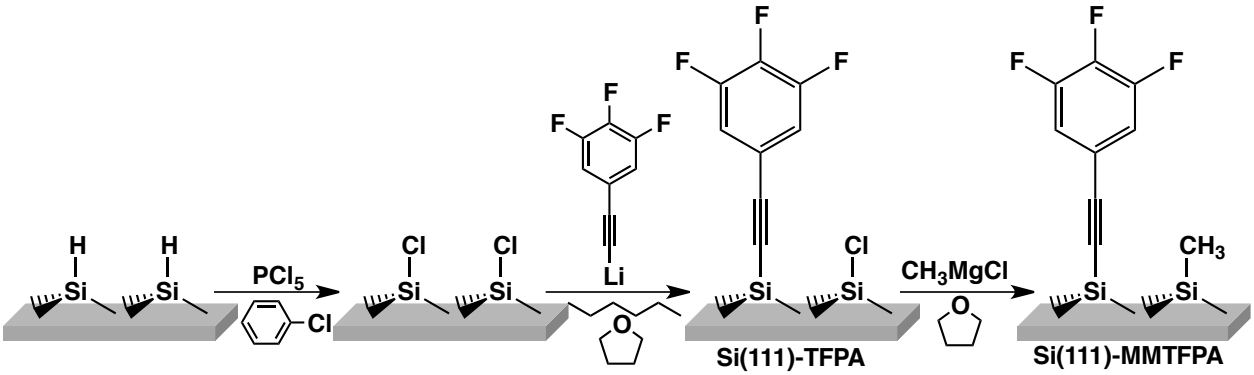

II.A.5. Formation of Ohmic Contacts to the Back of n- and p-Si(111) Electrodes. After functionalization, ohmic contacts were formed to the back of n-Si(111) electrodes by application of Ga-In eutectic (78% Ga, 22% In by weight) using a diamond-tipped scribe. Prior to functionalization, ohmic contacts were formed to p-Si(111) samples by electron-beam evaporation (Denton Vacuum) of 100 nm of Al onto the backside of the wafer.[47] The wafers were then annealed in a Carbolite tube furnace at 450 °C for 30 min under an atmosphere of forming gas (5% H_2(g) in N_2(g)) flowing at 5 L min^{-1}. The Al layer was isolated from reaction solutions during the functionalization process by use of a custom Teflon reaction vessel (Figure S1, Supporting Information).

II.A.6. Electrochemical Measurements in Contact with Hg. Electrochemical measurements in contact with Hg[40] (electronic grade 99.9999% trace metal basis, Sigma-Aldrich or Alfa Aesar) were performed inside an Ar(g)-filled glovebox (< 0.3 ppm O_2(g)) at 23 °C. The wafers were placed on a Cu plate (with the GaIn eutectic contacting the Cu plate), and a cylindrical Teflon cell was placed on top of the wafer, to produce an electrode area of 0.314 cm^2. Hg was added to the Teflon cell to cover the exposed area of the wafer, and a Pt wire contacted the top of the Hg. Electrochemical measurements were collected using a two-electrode setup, with the Cu plate connected to the working electrode and the Pt wire connected to the counter

electrode. All voltages measured in a 2-electrode setup are indicated by *V*, while potentials measured in a 3-electrode setup are indicated by *E*.

Current density versus voltage *(J-V)* measurements were performed from –0.5 to +0.5 V at a scan rate of 20 mV s^{-1}. The sampling rate was 1 mV per data point, using a Solartron 1287 potentiostat operated by CorrWare software (v. 3.2c). Three *J-V* scans were collected before and after collection of differential capacitance versus voltage (C_{diff}-*V*) data. C_{diff}-*V* data were acquired with a 10 mV amplitude sinusoidal signal at an applied DC bias, with the DC bias varied in increments of 0.05 V between 0 and +0.5 V for n-Si and between 0 and –0.5 V for p-Si electrodes. The frequency was varied from 10^1 to 10^6 Hz at each DC bias. C_{diff}-*V* measurements were collected using a Schlumberger SI 1260 frequency response analyzer operated by ZPlot software (v. 3.3e).

II.A.7. Photoelectrochemical Measurements in Acetonitrile. Si working electrodes were fabricated by using high-purity conductive Ag paint (SPI Supplies, West Chester, PA) to affix a coil of tinned Cu wire to the back side of the Si electrode. The wire was threaded through a ¼" outer diameter Pyrex tube, and the wafer was secured to the tube using Loctite 9460 epoxy (cured under ambient conditions for 12–24 h) such that the wafer surface was perpendicular to the length of the tube. Electrodes used for current density versus potential (*J-E)* and differential capacitance versus potential (C_{diff}-*E*) measurements were 0.14 to 0.61 cm^2 in area, as determined by analyzing scanned images of each electrode with ImageJ software. All *J-E* and C_{diff}-*E* measurements used a standard 3-electrode setup.

Decamethylferrocene (Cp^*_2Fe, bis(pentamethylcyclopentadienyl)iron(II), 99%) was purchased from Strem Chemical and was purified by sublimation. The oxidized decamethylferrocenium ($Cp^*_2Fe^+$, bis(pentamethylcyclopentadienyl)iron(III) tetrafluoroborate)

was synthesized by chemical oxidation of decamethylferrocene and purified by recrystallization from diethyl ether and acetonitrile.[48] Methyl viologen (MV^{2+}, 1,1'-dimethyl-4,4'-bipyridinium hexafluorophosphate) was prepared according to a literature procedure.[49] The reduced species $MV^{+\bullet}$ was generated by controlled-potential electrolysis of MV^{2+} at –0.85 V versus $AgNO_3$/Ag (Bioanalytical Systems, Inc.) with a Pt mesh working electrode in the main electrochemical cell compartment and a Pt mesh counter electrode located in a compartment that was separated from the main electrochemical cell by a Vycor frit. Subsequent *in situ* generation of the $MV^{+\bullet}$ species was performed to maintain the cell potential within 25 mV of the initial measured open-circuit potential versus a $AgNO_3$/Ag reference electrode.

Photoelectrochemical measurements were performed in acetonitrile (CH_3CN, EMD, dried over columns of activated alumina) with 1.0 M $LiClO_4$ (battery grade, Sigma-Aldrich) inside an Ar(g)-filled glovebox that contained <0.5 ppm of O_2(g). The concentrations of the redox-couple species in solution were either 1.2 mM $Cp^*_2Fe^+$ and 0.92 mM Cp^*_2Fe or were 1.5 mM MV^{2+} and 0.035 mM $MV^{+\bullet}$ (calculated based on charge passed during electrolysis). Initial open-circuit measurements were collected in the dark and also were collected under 100 mW cm^{-2} of illumination provided by a 300 W ELH-type tungsten-halogen lamp. The light intensity was calibrated by use of a Si photodiode (Thor Laboratories). *J-E* data were collected from –0.5 to +0.5 V versus a Pt wire pseudo-reference electrode in a three-electrode setup with a Pt mesh counter electrode, using a Gamry Reference 600 potentiostat operated by Gamry Instruments Framework software (v. 5.61). A four-port, cylindrical, flat-bottomed, borosilicate glass cell was used for the photoelectrochemical measurements. C_{diff}-*E* measurements were collected using a Gamry Reference 600 potentiostat with the same specifications used for the measurements performed in contact with Hg.

II.B. Instrumentation. *II.B.1. Transmission Infrared Spectroscopy.* TIRS data were collected using a Thermo Scientific Nicolet 6700 optical spectrometer[33] equipped with a thermoelectrically cooled deuterated L-alanine-doped triglycine sulfate (DLaTGS) detector, an electronically temperature-controlled (ETC) EverGlo mid-IR source, a N_2(g) purge, and a KBr beam splitter. A custom attachment allowed the wafers (1.3 × 3.2 cm) to be mounted with the incident IR beam at 74° (Brewster's Angle for Si) or 30° with respect to the surface normal. Spectra collected at 74° show modes that are either perpendicular or parallel to the surface, while spectra collected at 30° show primarily modes parallel to the surface.[50] The spectra reported herein are averages of 1500 scans at 4 cm^{-1} resolution. The baseline was flattened and the residual water peaks were subtracted in the reported spectra. Spectra were collected and processed using OMNIC software v. 9.2.41. The background SiO_x and Si(111)–H spectra were recorded separately for each sample.

II.B.2. X-ray Photoelectron Spectroscopy. XPS data were collected using a Kratos AXIS Ultra spectrometer.[7, 33, 51] The instrument was equipped with a hybrid magnetic and electrostatic electron lens system, a delay-line detector (DLD), and a monochromatic Al Kα X-ray source (1486.7 eV). Data were collected at pressures $<9 \times 10^{-9}$ Torr and the photoelectron ejection vector was 90° with respect to the sample surface plane. The electron-collection lens aperture was set to sample a 700 × 300 μm spot, and the analyzer pass energy was 80 eV for survey spectra and 10 eV for high-resolution spectra. The instrument energy scale and work function were calibrated using clean Au, Ag, and Cu standards. The instrument was operated by Vision Manager software v. 2.2.10 revision 5.

II.B.3. Surface Recombination Velocity. S measurements were performed using a contactless microwave conductivity apparatus.[7, 33-34, 43] A 20 ns laser pulse at 905 nm provided

by an OSRAM laser diode and an ETX-10A-93 driver generated electron-hole pairs. The charge-carrier lifetime was determined by monitoring the change in reflected microwave intensity using a PIN diode connected to an oscilloscope. The data were collected using a custom LabView program. All photoconductivity decay curves were averages of 64 consecutive decays. Reported data were collected after the *S* value had stabilized in the presence of air, usually 24–72 h after preparation of the surface.

II.C. Data Analysis. Detailed information for the fitting and quantification of XPS data, calculation of *S*, and analysis of *J*-*V*, *J*-*E*, C_{diff}-*V*, and C_{diff}-*E* data is presented in the Supporting Information.

II.C.1. Determination of the Effective Solution Potentials for Photoelectrochemical Cells. The Nernstian cell potential, $E(Cp^*_2Fe^{+/0})$, for $Cp^*_2Fe^{+/0}$ in CH_3CN with 1.0 M $LiClO_4$ was measured to be +0.023 V versus the formal potential of the redox couple, which is $E°'(Cp^*_2Fe^{+/0})$ = –0.468 V versus ferrocenium/ferrocene.[47] The reference potential was converted to the saturated calomel electrode (SCE) by use of the experimentally determined value of $E°'(Fc^{+/0})$ = +0.311 versus SCE.[47] $E(MV^{2+/+\bullet})$ for the $MV^{2+/+\bullet}$ in CH_3CN with 1.0 M $LiClO_4$ was measured as –0.781 V versus $AgNO_3$/Ag. The cell reference potential was converted to SCE using $E(AgNO_3/Ag)$ = +0.393 V versus SCE.[52] The measured cell potentials were converted to effective cell potentials, for which a normalizing 10 mM concentration was used for comparison with previous results. The effective cell potential for n-Si electrodes, $E_{eff,n}$ (A/A^-) was determined by:[47]

$$E_{\mathrm{eff,\,n}}\left(\mathrm{A}/\mathrm{A}^-\right) = E\left(\mathrm{A}/\mathrm{A}^-\right) + \frac{k_\mathrm{B}T}{q}\ln\frac{\left[\mathrm{A}^-_{\mathrm{eff}}\right]}{\left[\mathrm{A}^-\right]} \qquad (1)$$

and the effective cell potential for p-Si electrodes $E_{eff,p}$ (A/A^-) was determined by:

$$E_{\mathrm{eff,p}}\left(\mathrm{A}/\mathrm{A}^{-}\right) = E\left(\mathrm{A}/\mathrm{A}^{-}\right) - \frac{k_{\mathrm{B}}T}{q}\ln\frac{\left[\mathrm{A}_{\mathrm{eff}}\right]}{\left[\mathrm{A}\right]} \qquad (2)$$

Here, $\left[\mathrm{A}^{-}_{\mathrm{eff}}\right]$ and $\left[\mathrm{A}_{\mathrm{eff}}\right]$ are the effective 10 mM concentrations of the reduced and oxidized species, respectively, and $\left[\mathrm{A}^{-}\right]$ and $\left[\mathrm{A}\right]$ are the solution concentrations of the reduced and oxidized species, respectively. For the $Cp^{*}_{2}Fe^{+/0}$ cell, $E_{\mathrm{eff,n}}$ ($Cp^{*}_{2}Fe^{+/0}$) = –0.073 V versus SCE, and $E_{\mathrm{eff,p}}$ ($Cp^{*}_{2}Fe^{+/0}$) = –0.188 V versus SCE. For the $MV^{2+/+\bullet}$ cell, $E_{\mathrm{eff,n}}$ ($MV^{2+/+\bullet}$) = –0.244 V versus SCE, and $E_{\mathrm{eff,p}}$ ($MV^{2+/+\bullet}$) = –0.436 V versus SCE.

III. RESULTS

III.A. Spectroscopic Characterization and Surface Recombination Velocity of Si(111)–TFPA and Si(111)–MMTFPA Surfaces. Figure 2 presents TIRS data for a Si(111)–TFPA surface collected at 74° and 30° incidence with respect to the surface normal. The spectrum collected at 74° incidence exhibited an intense peak at 1533 cm^{-1}, which was ascribed to primary skeletal phenyl C–C stretching vibrations.[53-54] This peak was reduced in intensity at 30° incidence, indicating that this motion has a significant component that is perpendicular to the surface. At 74° incidence, weak peaks were observed at 1612, 1584, 1432, 1366, and 1351 cm^{-1} and were characteristic of aromatic systems.[54] At 30° incidence, the signal at 1432 cm^{-1} was readily observed, while the other characteristic aromatic C–C stretching peaks were not present. A sharp signal observed for 74° incidence at 1251 cm^{-1} was indicative of C–F stretching,[54-56] and this peak was greatly reduced in intensity at 30° incidence. A very weak signal at 2160 cm^{-1} was observed only at 74° incidence, indicating the presence of C≡C triple bond stretching perpendicular to the surface.[54] Weak C–H stretching signals were observed only for 74° incidence at 2962 and 2853 cm^{-1}, which can be ascribed to adventitious saturated hydrocarbon species.[50] No distinct aromatic C–H stretch (typically near 3050 cm^{-1}) signal was observed for

the surface-bound TFPA group. A broad peak centered near 1050 cm^{-1} was ascribed to transverse optical (TO) Si–O–Si stretching.[50] The observation of this mode indicated the presence of subsurface SiO_x, consistent with the oxidation of unreacted Si–Cl sites on the functionalized surface. A sharp signal overlapped by the Si–O–Si stretching peak was observed at both angles of incidence centered at 1055 cm^{-1} and was ascribed to in-plane aromatic C–H bending. No residual Si–H signal was detected when a SiO_x surface was used as a reference, indicating that the surface sites were only terminated by TFPA or Cl moieties.

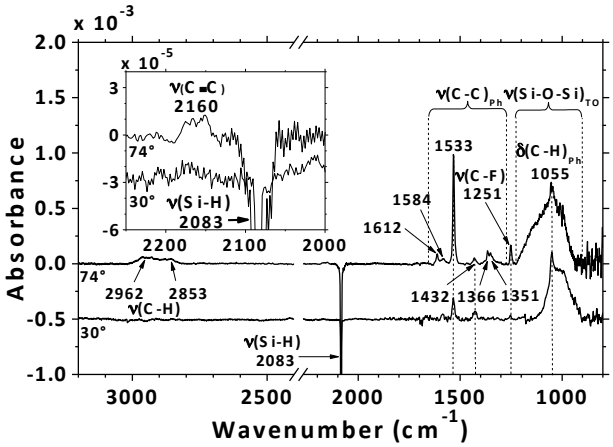

Figure 2. TIRS data for a Si(111)–TFPA surface collected at 74° (top) and 30° (bottom) with respect to the surface normal. The symbols ν and δ indicate stretching and bending motions, respectively, and the subscript "Ph" indicates modes associated with the phenyl ring. The spectrum collected at 74° had θ_{TFPA} = 0.16 ML and θ_{SiO_x} = 0.17 ML, while the spectrum collected at 30° had θ_{TFPA} = 0.25 ML and θ_{SiO_x} = 0.03 ML. The spectra were referenced to the Si(111)–H surface. The peak at 1533 cm^{-1} and the surrounding satellite peaks were attributed to skeletal C–C stretching in the phenyl ring. The C–F stretch was observed at 1251 cm^{-1}, and a weak C≡C stretch was observed at 2160 cm^{-1}. The inset shows a magnified portion of the spectrum from 2250 to 2000 cm^{-1}.

TIRS data for a Si(111)–MMTFPA sample with θ_{TFPA} = 0.16 ML are presented in Figure S2 (Supporting Information). The Si(111)–MMTFPA surface showed the modes associated with the phenyl ring and aromatic C–F stretching observed in Figure 2 in addition to reduced SiO_x content. The symmetric C–H bending, δ_s(C–H),[50] mode overlapped significantly with the C–F stretching peak, resulting in a single peak at 1253 cm^{-1}. Additionally, the $–CH_3$ rocking mode was observed at 762 cm^{-1}.[50] The presence of these peaks demonstrates that the Si(111)–MMTFPA exhibits both TFPA and $–CH_3$ functionality.

Figure 3 shows the surface recombination velocity (S) as a function of the composition of the functionalized Si surfaces. The Si(111)–CH_3 surface exhibited S = 13 ± 5 cm s^{-1}, which corresponds to a trap-state density, N_t, of ~1.3 × 10^9 cm^{-2}, i.e. 1 trap for every 6.0 × 10^5 surface sites. This low trap-state density has been shown to be stable over >500 h of air exposure.[32-33] A substantial increase in S was observed for surfaces with θ_{TFPA} > 0.1 ML, which is consistent with an increase in S observed for increased fractional coverages of bulky groups in mixed monolayers on Si(111) surfaces.[34, 43] A Si(111)–MMTFPA surface with θ_{TFPA} = 0.10 ML exhibited S = (1.6 ± 0.5) × 10^2 cm s^{-1}, corresponding to N_t =1.6 × 10^{10} cm^{-2}. With θ_{TFPA} = 0.22 ML, a Si(111)–MMTFPA surface had S = (1.9 ± 0.1) × 10^3 cm s^{-1}, corresponding to N_t = 1.9 × 10^{11} cm^{-2}. The Si(111)–TFPA surface, which had higher θ_{TFPA} than the measured Si(111)–MMTFPA samples, exhibited substantially higher S than was observed for the measured Si(111)–MMTFPA.

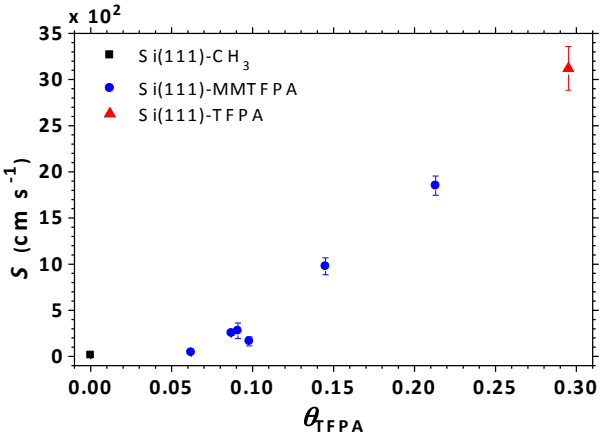

Figure 3. *S* values for Si(111)–CH_3, Si(111)–MMTFPA, and Si(111)–TFPA surfaces as a function of fractional monolayer coverage with TFPA groups. For $\theta_{TFPA} > 0.1$ ML, *S* increased rapidly.

Figure 4a presents a representative XP survey spectrum of a Si(111)–MMTFPA surface with $\theta_{TFPA} = 0.11$ ML. Survey spectra were free of contaminants and only showed the presence of Si, C, O, and F core-level peaks. A high-resolution C 1s spectrum showed the presence of C bound to Si at 284.2 eV,[33, 41, 57] C bound to C at 285.3 eV, C bound to O at 286.8 eV, and C bound to F at 288.0 eV (Figure 4b).[45, 58-59] Figure 4c shows the high-resolution Si 2p XP spectrum, which showed only bulk Si^0 and no detectable high-order SiO_x in the 102–104 eV region. The F 1s high-resolution spectrum exhibited a single peak at 688.3 eV (Figure 4d), indicative of a single source of F on the surface.[59] Generally, samples with $\theta_{TFPA} < 0.15$ ML exhibited no detectable SiO_x in the 102–104 eV range, while samples with $\theta_{TFPA} > 0.15$ ML exhibited $\theta_{SiO_x} = 0.07 \pm 0.02$ ML. Samples with $\theta_{TFPA} > 0.2$ ML also often exhibited a small amount of residual Cl, which gave an average Si–Cl coverage, θ_{Cl}, of 0.11 ± 0.01 ML.

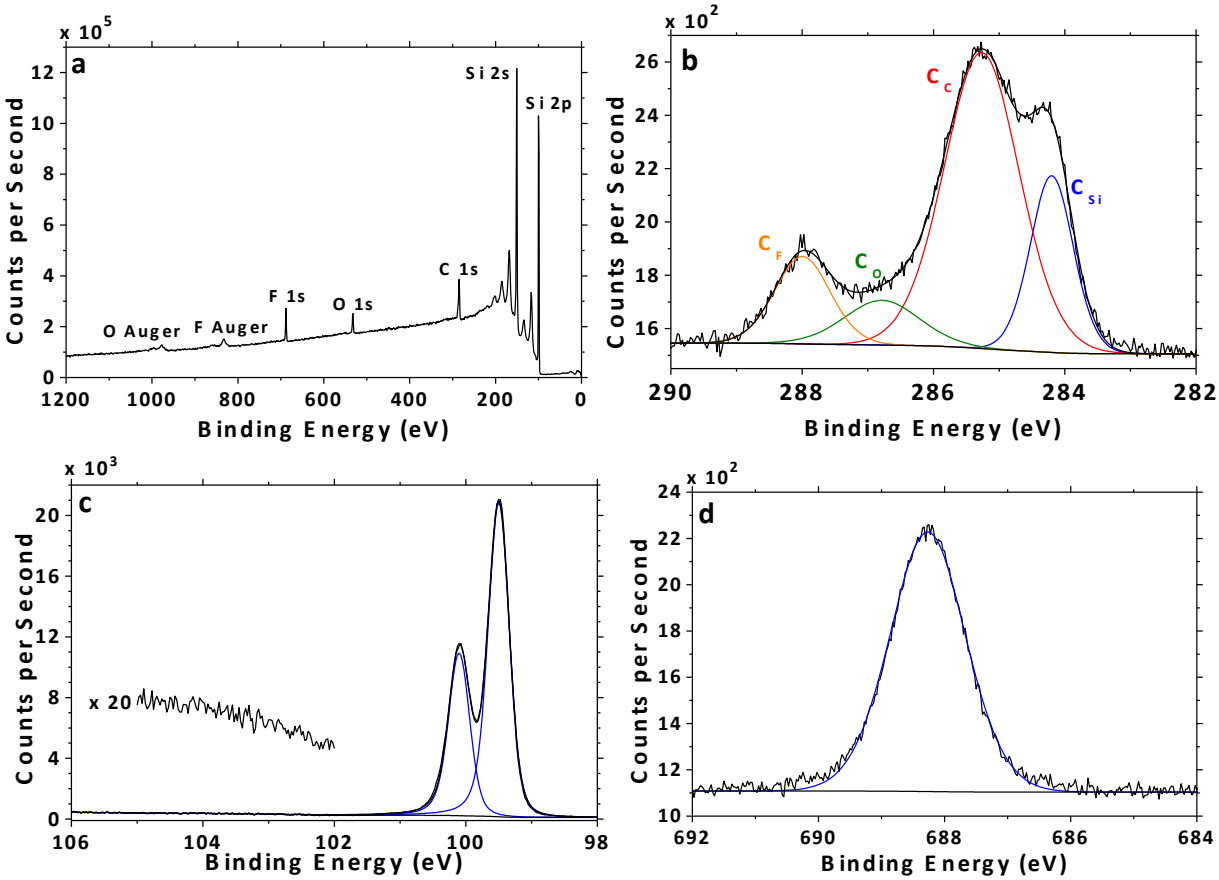

Figure 4. XPS data for an n-Si(111)–MMTFPA surface with θ_{TFPA} = 0.11 ML. The survey spectrum (a) exhibited signals from Si, C, O, and F. The high-resolution C 1s spectrum (b) showed signals ascribed to C bound to Si (C_{Si}), C bound to C (C_C), C bound to O (C_O), and C bound to F (C_F). The Si 2p high-resolution spectrum (c) showed peaks attributed to bulk Si^0 with no detectable high-order SiO_x (magnified region). The F 1s high-resolution spectrum (d) exhibited a single peak ascribed to F bound to C.

Figure S3 (Supporting Information) shows analogous XP spectra for a Si(111)–TFPA surface with θ_{TFPA} = 0.35 ML. Without subsequent methylation, the Si(111)–TFPA surface exhibited residual Cl, as seen in the survey spectrum (Figure S2a) and in the high-resolution Cl 2s spectrum (Figure S2e). The C 1s spectrum similarly showed contributions from C bound to Si

(284.1 eV), C bound to C (285.0 eV), C bound to O (286.2 eV), and C bound to F (287.6 eV) (Figure S2b). The Si 2p spectrum shown did not exhibit detectable levels of SiO_x, while θ_{SiO_x} = 0.11 ± 0.07 ML across multiple Si(111)–TFPA sample preparations (Figure S2c). The F 1s spectrum exhibited a single signal centered at 687.9 eV (Figure S2d).

III.B. Hg Contacts to Si(111)–MMTFPA Surfaces. Figure 5a displays the *J-V* behavior for n-Si(111)–MMTFPA/Hg contacts having a range of θ_{TFPA}. By convention, measured values of Φ_b and of the built-in voltage were unsigned for two-electrode measurements in contact with Hg. The n-Si(111)–CH_3/Hg contact exhibited strongly rectifying behavior (Φ_b = 0.9 V), evidenced by small, near-constant current at reverse bias.[40] The n-Si(111)–MMTFPA/Hg contacts exhibited less rectification as θ_{TFPA} increased, suggesting that the molecular dipole induced by the C–F bonds in the TFPA group shifted the band-edge positions to produce a smaller built-in voltage at the n-Si(111)–MMTFPA/Hg junction. At high θ_{TFPA}, the n-Si–MMTFPA/Hg contact was ohmic to Hg, indicating $\Phi_b \leq 0.3$ V and corresponding to a shift of ≥0.6 V in the Si band-edge positions compared with n-Si(111)–CH_3 surfaces. Samples that exhibited low values for Φ_b generally did not exhibit clear linear regions in the forward-bias portion of the semi-log *J-V* plot, which precluded analysis of the *J-V* data within a thermionic emission model. The diode-ideality factor, *n*, for the n-Si(111)–MMTFPA/Hg junctions was estimated as 1.5 ± 0.2 (eq S4), which is comparable to previous observations on junctions between alkyl-terminated n-Si and Hg.[40]

Figure 5b shows *J-V* data for p-Si(111)–MMTFPA surfaces in contact with Hg. The p-Si(111)–CH_3 samples exhibited ohmic behavior in contact with Hg, and previous work has indicated that $\Phi_b < 0.15$ V for this junction.[40] Addition of TFPA to the alkyl monolayer resulted in increased rectification of the junction, producing measureable values for Φ_b. Similar to n-

Si/Hg junctions, p-Si/Hg junctions that exhibited low values for Φ_b gave semi-log *J-V* response curves with no definitive linear portion in the forward-bias region, thereby limiting the determination of Φ_b for these samples. The p-Si(111)–MMTFPA samples showed increased rectification with increasing θ_{TFPA}, which indicated an increase in the built-in voltage for p-Si/Hg junctions as θ_{TFPA} increased. Analysis of the *J-V* response yielded a maximum measured value for Φ_b of 0.7 V on p-Si(111)–MMTFPA/Hg junctions, which indicated a shift in the band-edge positions of ≥0.5 V relative to p-Si(111)–CH_3 surfaces. The value of n for p-Si(111)–MMTFPA/Hg junctions was 1.3 ± 0.2 (eq S4).

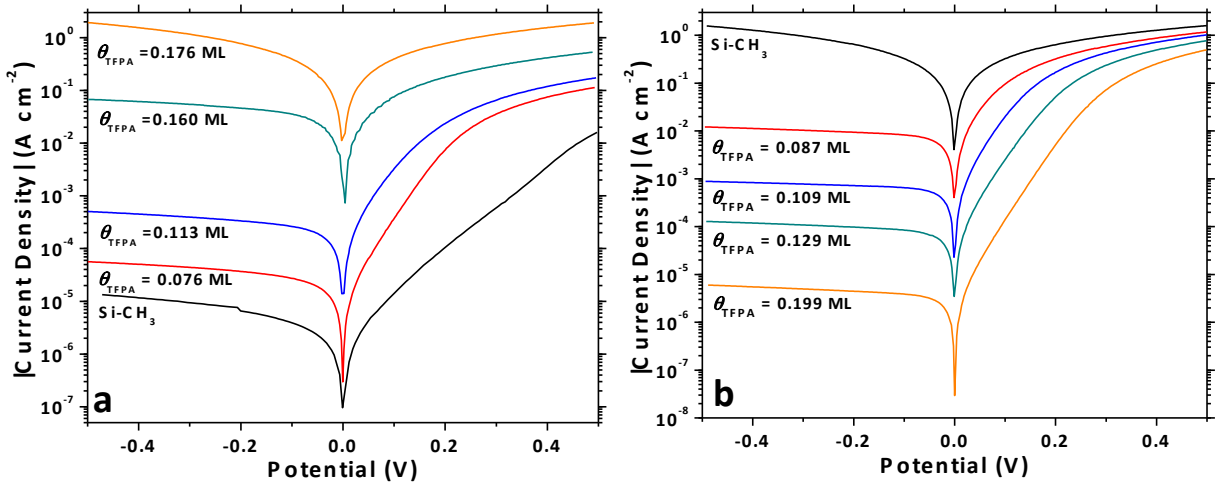

Figure 5. Representative two-electrode *J-V* behavior for (a) n-type and (b) p-type Si(111)–MMTFPA/Hg junctions. The fractional ML coverage of TFPA for a given curve is indicated below each curve. By convention, the forward bias region is depicted in the first quadrant.

C_{diff}-*V* data were also collected for the functionalized n-Si/Hg and p-Si/Hg junctions. The flat-band position was calculated from the C_{diff}-*V* data using eq S5, and the flat-band values were used to determine Φ_b (eq S6 or eq S7). As with *J-V* measurements, samples with small Φ_b in contact with Hg generally did not exhibit ideal behavior by C_{diff}-*V* measurements, precluding determination of Φ_b for samples that did not show strong rectification. The dopant density, N_D,

was also calculated from these measurements and was compared to the value of N_D determined by 4-point probe measurements. For n-Si, N_D determined by C_{diff}-V analysis was (2.7 ± 0.3) × 10^{15} cm^{-3}, and N_D determined by 4-point probe data was 4.4 × 10^{15} cm^{-3}. For p-Si, N_D determined by C_{diff}-V analysis was (1.7 ± 0.4) × 10^{16} cm^{-3}, and 4.0 × 10^{16} cm^{-3} by 4-point probe. For either n-Si and p-Si samples, the values of N_D were thus within a factor of ~2 when calculated by the C_{diff}-V or by 4-point probe measurements.

Figure 6 presents the values of Φ_b calculated from the J-V response and C_{diff}-V analysis for Si(111)–MMTFPA/Hg junctions as a function of θ_{TFPA}. The n-Si(111)–MMTFPA/Hg junctions exhibited values of Φ_b that were in close agreement for both methods. Samples for which the junction appeared ohmic are plotted with a value of Φ_b = 0 V. The p-Si(111)–MMTFPA/Hg junctions showed values of Φ_b that generally were not in good agreement for the two analytical methods used, and Φ_b determined by C_{diff}-V measurements exhibited significantly greater spread for a given θ_{TFPA} than Φ_b determined from J-V measurements. For high θ_{TFPA}, the p-Si/Hg junctions exhibited values of Φ_b determined by Mott-Schottky analysis near the Si band gap, while apparent Φ_b values determined from analysis of the J-V response were considerably lower, at ~0.65 V.

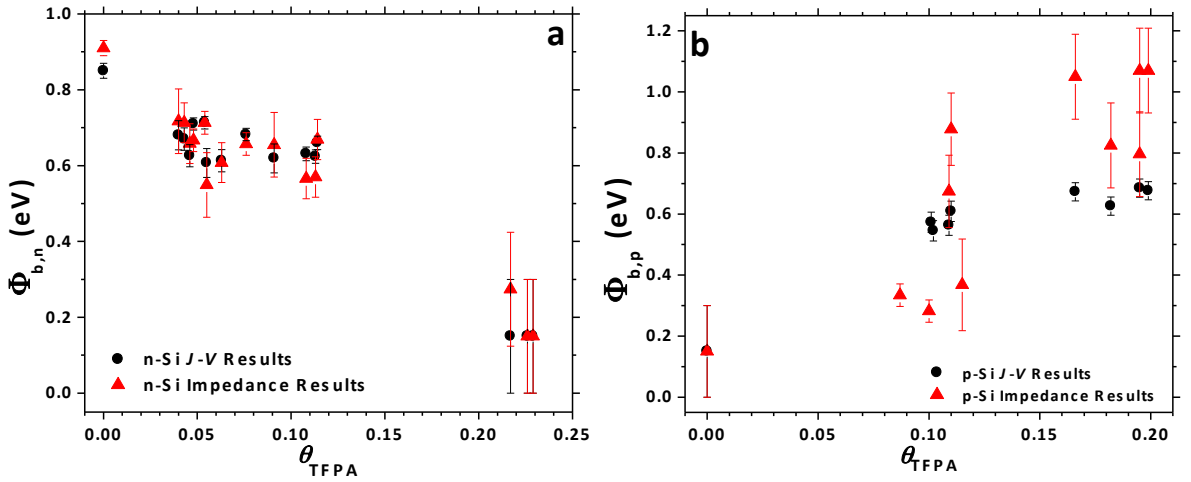

Figure 6. Correlation between the calculated barrier height for Si(111)–MMTFPA/Hg junctions and the fractional monolayer coverage of TFPA for (a) n-type and (b) p-type samples. The barrier heights calculated from fitting the forward bias region of the *J-V* curves using eq S4 are shown as black circles, and the barrier heights calculated from fitting the C_{diff}-*V* data using eqs S5, S6, and S7 are shown as red triangles. Samples that showed low Φ_b values did not exhibit ideal junction behavior, precluding analysis of Φ_b for samples with poor rectification. Error bars represent the statistical variation in Φ_b for samples from the same preparation.

III.C. Photoelectrochemical Behavior of Si(111)–TFPA and Si(111)–MMTFPA Surfaces in Contact with CH_3CN-$Cp^*_2Fe^{+/0}$. Figure 7 presents representative *J-E* data for functionalized n- and p-Si(111) samples in contact with CH_3CN-$Cp^*_2Fe^{+/0}$ (1.2, 0.92 mM) under 100 mW cm^{-2} of simulated solar illumination. The effective cell potential, $E_{eff}(Cp^*_2Fe^{+/0})$, was determined using eq 1 and eq 2, to give $E_{eff,n}(Cp^*_2Fe^{+/0})$ = –0.073 V and $E_{eff,p}(Cp^*_2Fe^{+/0})$ = –0.188 versus SCE. Data for the Si(111)–CH_3 surface were collected for comparison with Si(111)–MMTFPA and Si(111)–TFPA samples. The photocurrent density was limited by mass transport because the electrode areas were relatively large and the redox couple concentrations were low. Large electrode areas were required to produce reliable C_{diff}-*E* measurements with minimal edge effects. Table 1 presents the measured values of the open circuit potential (E_{oc}) for

the functionalized electrodes under 100 mW cm^{-2} illumination as well as the values of Φ_b determined from C_{diff}-E measurements. Values of Φ_b are reported as unsigned magnitudes.

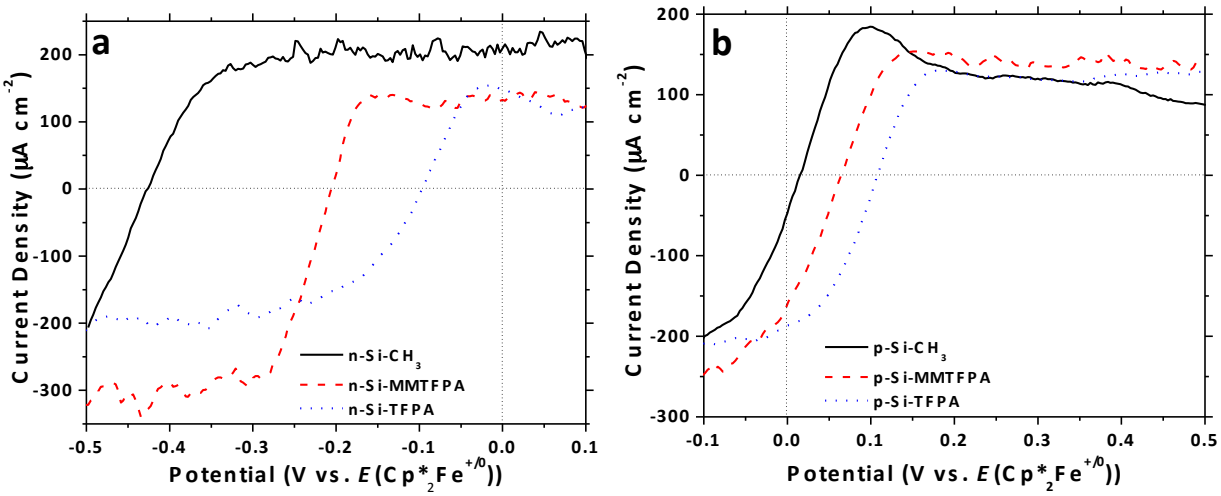

Figure 7. Representative *J*-*E* data under 100 mW cm^{-2} simulated sunlight illumination for functionalized Si(111) surfaces in contact with $Cp^*_2Fe^{+/0}$ (1.2, 0.92 mM) in dry CH_3CN for (a) n-type and (b) p-type samples. Si(111)–CH_3 samples (solid black) are shown for comparison with Si(111)–MMTFPA (dashed red) and Si(111)–TFPA (blue dotted) samples.

Table 1. E_{oc} and Φ_b measurements for functionalized Si surfaces in contact with CH_3CN-$Cp^*_2Fe^{+/0}$.

Surface	E_{oc} in $Cp^*_2Fe^{+/0}$ (V)[a]	Φ_b in $Cp^*_2Fe^{+/0}$ (V)[b]	θ_{TFPA} (ML)
n-Si–CH_3	–0.43 ± 0.02	1.07	0
n-Si–MMTFPA	–0.16 ± 0.03	0.56 ± 0.01	0.23 ± 0.01
n-Si–TFPA	–0.072 ± 0.001	0.427 ± 0.001	0.307 ± 0.007
p-Si–CH_3	+0.03 ± 0.03	-	0
p-Si–MMTFPA	+0.095 ± 0.004	0.56 ± 0.07	0.193 ± 0.007
p-Si–TFPA	+0.12 ± 0.02	0.35 ± 0.01	0.27 ± 0.02

[a]The redox couple concentrations were 1.2 mM $Cp^*_2Fe^+$ and 0.92 mM Cp^*_2Fe. The effective cell potentials calculated from eq 1 and eq 2 were $E_{eff,n}$ ($Cp^*_2Fe^{+/0}$) = –0.073 V and $E_{eff,p}$ ($Cp^*_2Fe^{+/0}$) = –0.188 V versus SCE. [b]The values of Φ_b were determined by C_{diff}-E measurements using eq S8 through S11 and are reported as unsigned magnitudes. No value for Φ_b is reported for samples that formed weakly rectifying junctions with the redox solution.

The E_{oc} of n-Si(111)–MMTFPA and n-Si(111)–TFPA samples shifted by +0.27 V and +0.36 V, respectively, compared with the E_{oc} for n-Si(111)–CH_3 samples in contact with CH_3CN-$Cp^*_2Fe^{+/0}$. The calculated values of Φ_b for n-Si(111)–MMTFPA and n-Si(111)–TFPA samples were lowered in magnitude by 0.51 V and 0.64 V, respectively, compared with Φ_b for n-Si(111)–CH_3 samples in contact with CH_3CN-$Cp^*_2Fe^{+/0}$. The dopant density, N_D, for functionalized n-Si samples was found to be $(4.6 \pm 0.8) \times 10^{15}$ cm^{-3}, which agreed well with N_D determined from 4-point probe measurements (4.4×10^{15} cm^{-3}).

For p-Si samples in contact with CH_3CN-$Cp^*_2Fe^{+/0}$, the E_{oc} shifted positively and Φ_b increased in magnitude for surfaces that contained TFPA functionality compared with p-Si(111)–CH_3 surfaces. The p-Si(111)–CH_3 samples exhibited very low photovoltages, and Φ_b was too small to be accurately determined by C_{diff}-E measurements. The p-Si(111)–MMTFPA samples exhibited a moderate shift in E_{oc} of +0.07 V relative to p-Si(111)–CH_3 samples, and p-Si(111)–TFPA samples showed a slightly greater shift in E_{oc} of +0.09 V. The p-Si(111)–MMTFPA samples yielded $\Phi_b = 0.56 \pm 0.07$ V, while p-Si(111)–TFPA samples yielded an apparent Φ_b of 0.35 ± 0.01 V despite the higher E_{oc} observed for these samples relative to p-Si(111)–MMTFPA samples. The value of N_D determined from C_{diff}-E measurements in contact with CH_3CN-$Cp^*_2Fe^{+/0}$ was $2.0 \pm 0.3 \times 10^{16}$ cm^{-3}, compared with the value of $N_D = 4.0 \times 10^{16}$ cm^{-3} determined from 4-point probe measurements.

III.D. Photoelectrochemical Behavior of Si(111)–TFPA and Si(111)–MMTFPA Surfaces in Contact with CH_3CN-$MV^{2+/+\bullet}$. Figure 8 shows representative J-E data for functionalized n- and p-Si(111) samples in contact with CH_3CN-$MV^{2+/+\bullet}$ (1.5, 0.035 mM) under 100 mW cm^{-2} simulated solar illumination. The effective cell potential, $E_{eff}(MV^{2+/+\bullet})$ was determined using eq 1 and eq 2 to give $E_{eff,n}(MV^{2+/+\bullet}) = -0.244$ V and $E_{eff,p}(MV^{2+/+\bullet}) = -0.436$ V versus SCE. Low concentrations (0.035 mM) of the radical $MV^{+\bullet}$ species resulted in very low anodic photocurrent densities. Table 2 presents the measured values of E_{oc} determined for the functionalized electrodes under 100 mW cm^{-2} illumination, in addition to the absolute values of Φ_b determined from C_{diff}-E measurements.

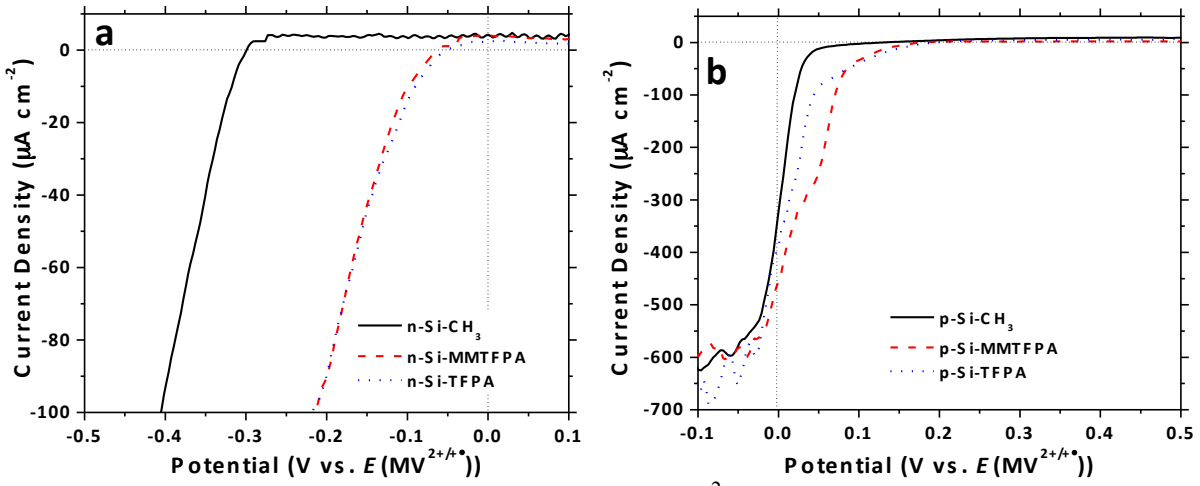

Figure 8. Representative *J-E* data under 100 mW cm^{-2} illumination for functionalized Si(111) surfaces in contact with $MV^{2+/+\bullet}$ (1.5, 0.035 mM) in dry CH_3CN for (a) n-type and (b) p-type samples. Si(111)–CH_3 samples (solid black) are shown for comparison with Si(111)–MMTFPA (dashed red) and Si(111)–TFPA (blue dotted) samples.

Table 2. E_{oc} and Φ_b measurements for functionalized Si surfaces in contact with CH_3CN-$MV^{2+/+\bullet}$.

Surface	E_{oc} in $MV^{2+/+\bullet}$ (V)[a]	Φ_b in $MV^{2+/+\bullet}$ (V)[b]	θ_{TFPA} (ML)
n-Si–CH_3	–0.26 ± 0.02	0.64 ± 0.06	0
n-Si–MMTFPA	–0.021 ± 0.007	-	0.23 ± 0.01
n-Si–TFPA	–0.01 ± 0.01	-	0.310 ± 0.007
p-Si–CH_3	+0.15 ± 0.01	0.51 ± 0.08	0
p-Si–MMTFPA	+0.254 ± 0.009	0.99 ± 0.07	0.196 ± 0.002
p-Si–TFPA	+0.24 ± 0.02	0.7 ± 0.1	0.26 ± 0.02

[a]The redox couple concentrations were 1.5 mM MV^{2+} and 0.035 mM $MV^{+\bullet}$. The effective cell potentials calculated from eq 1 and eq 2 were $E_{eff,n}$ ($MV^{2+/+\bullet}$) = –0.244 V and $E_{eff,p}$ ($MV^{2+/+\bullet}$) =

–0.436 V versus SCE. [b]The values of Φ_b were determined by C_{diff}-E measurements using eq S8 through S11 and are reported as unsigned magnitudes. No value for Φ_b is reported for samples that formed weakly rectifying junctions with the redox solution.

The E_{oc} of n-Si(111)–MMTFPA samples in contact with CH_3CN-$MV^{2+/+\bullet}$ shifted by +0.24 V relative to the E_{oc} of n-Si(111)–CH_3 samples. This shift is comparable to the shift observed for the same samples in contact with CH_3CN-$Cp^*_2Fe^{+/0}$. The n-Si(111)–TFPA samples in contact with CH_3CN-$MV^{2+/+\bullet}$ exhibited a slightly larger shift in $E_{oc,}$ of +0.25 V, compared to the E_{oc} for n-Si(111)–CH_3 samples. The value of Φ_b for n-Si(111)–CH_3 samples in contact with CH_3CN-$MV^{2+/+\bullet}$ was 0.64 ± 0.06 V, while the low barrier at n-Si(111)–MMTFPA and n-Si(111)–TFPA junctions with CH_3CN-$MV^{2+/+\bullet}$ precluded determination of Φ_b by C_{diff}-E measurements. The change in measured E_{oc} and Φ_b for n-Si samples containing TFPA functionality is consistent with an overall positive shift in the composite molecular dipole present at the interface. The dopant density, N_D, for functionalized n-Si samples was found to be (4.7 ± 0.2) × 10^{15} cm^{-3} in contact with CH_3CN-$MV^{2+/+\bullet}$.

As observed for p-Si samples in contact with CH_3CN-$Cp^*_2Fe^{+/0}$, the E_{oc} for p-Si(111)–MMTFPA and p-Si(111)–TFPA samples in contact with CH_3CN-$MV^{2+/+\bullet}$ shifted positively relative to E_{oc} for p-Si(111)–CH_3 surfaces. The positive shift in E_{oc} was accompanied by an increase in the magnitude of Φ_b. The p-Si(111)–MMTFPA samples exhibited a modest shift in $E_{oc,}$ of +0.10 V in contact with $MV^{2+/+\bullet}$ relative to the E_{oc} of p-Si(111)–CH_3 samples, and p-Si(111)–TFPA samples showed a very similar shift in E_{oc} of +0.09 V relative to p-Si(111)–CH_3 samples. For p-Si(111)–CH_3 samples, Φ_b was determined by C_{diff}-E measurements to be 0.51 ± 0.08 V, while Φ_b = 0.99 ± 0.07 V for p-Si(111)–MMTFPA surfaces, i.e. the barrier height of this

junction is close to the Si band gap. As was observed in contact with $Cp^*_2Fe^{+/0}$, p-Si(111)–TFPA samples yielded a lower Φ_b of 0.7 ± 0.1 V, despite the nearly identical E_{oc} observed for these samples as compared to p-Si(111)–MMTFPA samples. The value of N_D determined from C_{diff}-E measurements was $(2.4 \pm 0.4) \times 10^{16}$ cm^{-3}.

IV. DISCUSSION

IV.A. Si(111)–TFPA Surface Characterization. The TIRS data for Si(111)–TFPA surfaces yielded modes consistent with the presence of a phenyl ring, aryl C–F bonds, and a C≡C bond (Figure 2). The observation of the C≡C stretch at 2160 cm^{-1} at 74° incidence but not at 30° incidence indicates that TFPA group is predominantly oriented perpendicular to the surface. The large reduction in intensity of the primary aromatic C–C stretching peak at 1533 cm^{-1} at 30° incidence relative to 74° incidence demonstrates that this mode is primarily oriented perpendicular to the surface. Similarly, the C–F stretching signal at 1251 cm^{-1} was greatly reduced at 30° incidence relative to 74° incidence, indicating that the majority of this mode is oriented perpendicular to the surface. The residual intensity observed for the 1533 and 1251 cm^{-1} modes at 30° incidence indicates that a fraction of each mode is not perpendicular to the surface, in accord with expectations based on the geometry of the TFPA group. The in-plane aromatic C–H bend was observed at both angles of incidence at 1055 cm^{-1}, indicating that this mode is not primarily oriented perpendicular to the surface. The aryl C–H stretching peaks near 3050 cm^{-1} were not observed by TIRS, suggesting that substitution of the phenyl group with C–F bonds weakens the C–H stretching signal for the TFPA group.

TIRS data for the Si(111)–MMTFPA surface, presented in Figure S2, showed a single peak at 1253 cm^{-1} that was ascribed to the overlap of the symmetric C–H bending and C–F stretching modes. The energy of this mode falls between the TFPA C–F stretch, observed at

1251 cm^{-1}, and the symmetric C–H bend of the $–CH_3$ group, observed at 1257 cm^{-1}.[50] The Si(111)–TFPA sample exhibited a 0.18 height ratio of the peak at 1253 cm^{-1} relative to the peak at 1533 cm^{-1}, while the Si(111)–MMTFPA sample yielded a 0.22 height ratio of the peak at 1251 cm^{-1} relative to the peak at 1533 cm^{-1}. Thus, the peak at 1253 cm^{-1} on the Si(111)–MMTFPA sample results from a convolution of the symmetric C–H bending and C–F stretching modes, indicating that both TFPA and $–CH_3$ groups are present on the surface.

The shoulder observed in the C 1s XPS signal of the Si(111)–TFPA surface (Figure S2b) centered at 284.1 eV provides evidence for the formation of a Si–C bond. The residual Cl observed on Si(111)–MMTFPA surfaces for samples with $\theta_{TFPA} > 0.2$ ML is consistent with steric crowding of the surface precluding reaction of a small fraction of residual Si–Cl sites with CH_3MgCl. This behavior suggests considerable steric crowding that limited further passivation of the remaining Si–Cl sites on surfaces with $\theta_{TFPA} > 0.2$ ML.

A small amount of SiO_x was observed in the Si 2p spectrum from 102–104 eV on Si(111)–MMTFPA surfaces containing $\theta_{TFPA} > 0.15$ ML and on Si(111)–TFPA surfaces. Mixed monolayers with high concentrations of bulky groups can prevent passivation of neighboring Si–Cl sites with $–CH_3$ groups for steric reasons, leaving the surface sites more susceptible to oxidation.[34] Consistently, slightly more SiO_x was observed on Si(111)–TFPA surfaces compared with Si(111)–MMTFPA surfaces with high θ_{TFPA}.

Si(111)–MMTFPA samples exhibited high *S* compared with previously reported mixed monolayers.[7, 34, 43] A discussion of the relationship between the reagents used to prepare the mixed monolayers and the resulting *S* is presented in the Supporting Information.

IV.B. Hg Contacts to Si(111)–MMTFPA Surfaces. The work function of Hg is 4.49 eV,[60] which lies between the energies of the bottom of the conduction band and the top of the

valence band of bulk Si, and is very near the estimated energy of the absolute electrochemical potential for the standard hydrogen electrode (SHE), which is 4.44 eV at 25 °C.[61-62] Hg can also be readily applied to and removed from the Si surface at room temperature without formation of metal silicides.[40]

The *J-V* data presented in Figure 5, and the plots of Φ_b versus θ_{TFPA} in Figure 6, show a clear trend in the value of Φ_b as a function of θ_{TFPA} for functionalized n- and p-Si(111) surfaces in contact with Hg. The surface composition played an essential role in the electrical behavior of the junction. The composite dipole at the interface between the Si and the Hg results in a net electric field that can be tuned to energetically favor the transfer of electrons from p-Si to Hg or holes from n-Si to Hg, respectively. The n-Si/Hg junction exhibited maximum rectification for surfaces terminated by $–CH_3$ groups, and addition of TFPA to the monolayer yielded junctions with lower Φ_b. The decrease in Φ_b with increase in θ_{TFPA} resulted from a shift in the band-edge positions. The electrical behavior of n-Si(111)–MMTFPA/Hg junctions that showed ohmic behavior by *J-V* analysis could have also been influenced by high surface recombination velocity, which was measured for samples with high θ_{TFPA}.

For p-Si, the Si(111)–CH_3 surface formed an ohmic contact with Hg, and addition of TFPA to the monolayer resulted in an increase in Φ_b as θ_{TFPA} increased. Hence as θ_{TFPA} increased the band-edge positions of the Si shifted relative to the band-edge positions of Si(111)–CH_3 surfaces. This behavior is consistent with the formation of a surface dipole in the orientation shown in Figure 1b due to the addition of surficial TFPA. The resulting electric field at the interface is favorable for the flow of electrons from p-Si to the Hg contacting phase.

The values of Φ_b for Hg contacts to n-Si electrodes determined by *J-V* analysis agreed well with those obtained by C_{diff}-*V* analysis. In contrast, C_{diff}-*V* analysis for p-Si/Hg contacts

with θ_{TFPA} near 0.2 ML yielded Φ_b = 1.07 V, i.e. close to the Si band gap, while *J-V* data of the same samples yielded Φ_b = 0.68 V. The C_{diff}-*V* analysis is performed while the sample is in reverse bias and passes only small amounts of current to measure the real and imaginary impedance as well as the current-voltage phase shift. C_{diff}-*V* analysis thus minimizes the effects of recombination current on the calculated Φ_b. *J-V* analysis, in contrast, is performed in forward bias, for which significantly more current passes, and the effects of surface recombination are more readily observed. The difference in Φ_b determined for p-Si(111)–MMTFPA/Hg by *J-V* versus C_{diff}-*V* methods indicates that high *S* values yields lower Φ_b when measured by *J-V* analysis.

Si(111)–H surfaces have been widely used for fabrication of Si-based optoelectronic devices, and comparison of the band-edge positions of Si(111)–H surfaces with the results reported in this work is informative. For n-Si, the electrical behavior of Si(111)–H surfaces in contact with Hg produced a junction with Φ_b = 0.3 V, which appeared ohmic when measured at 296 K.[40] The n-Si(111)–MMTFPA samples with θ_{TFPA} > 0.17 ML in contact with Hg produced behavior similar to the n-Si(111)–H samples. Previous results for p-Si(111)–H/Hg junctions yielded Φ_b = 0.8 V by both *J-V* and C_{diff}-*V* measurements,[40] while p-Si(111)–MMTFPA samples achieved a maximum Φ_b of 0.68 V when measured by *J-V* analysis. The near-band-gap Φ_b measured by C_{diff}-*V* analysis for p-Si(111)–MMTFPA samples indicated that the band-edge positions were energetically closer to the vacuum level than the band-edge positions of Si(111)–H surfaces, but high *S* values for these surfaces limited the Φ_b measured under *J-V* operation.

IV.C. Photoelectrochemical Measurements of Si(111)–TFPA and Si(111)–MMTFPA Surfaces in CH_3CN. Photoelectrochemical measurements for n- and p-Si(111)–CH_3 samples in contact with CH_3CN-$Cp^*_2Fe^{+/0}$ were in good agreement with previously reported results.[47]

However, n- and p-Si(111)–CH_3 samples in contact with CH_3CN-$MV^{2+/+\bullet}$ exhibited E_{oc} values of –0.26 ± 0.02 and +0.15 ± 0.01 V, respectively that were not within the error of previously reported results of –0.10 ± 0.03 V and +0.31 ± 0.02 V, respectively.[47] The calculated values of $E_{eff,n}$ ($MV^{2+/+\bullet}$) and $E_{eff\,p}$ ($MV^{2+/+\bullet}$) were shifted by –0.16 V and –0.13 V, respectively, compared to previous work. This difference in effective solution potential likely arose because the previous work used 1,1'-dimethyl-4,4'-bipyridinium dichloride hydrate as the source of MV^{2+}, while this work used 1,1'-dimethyl-4,4'-bipyridinium hexafluorophosphate. The reversible potential for the $MV^{2+/+\bullet}$ couple has previously been found to be dependent on the nature of the anion in the electrolyte.[63] For the calculated values of $E_{eff,n}$ (A/A^-) and $E_{eff,p}$ (A/A^-), extrapolation of the results reported previously predicts E_{oc} values that are within close agreement with the values measured in this work.

Photoelectrochemical measurements under 100 mW cm^{-2} illumination demonstrated that the E_{oc} exhibited by the semiconductor-liquid junctions was sensitive to the surface composition. Compared with Si(111)–CH_3 samples, E_{oc} for n-Si(111)–MMTFPA samples shifted by +0.27 V in contact with CH_3CN-$Cp^*_2Fe^{+/0}$ and by +0.24 V in contact with CH_3CN-$MV^{2+/+\bullet}$. The n-Si(111)–TFPA samples exhibited a greater shift in E_{oc}, suggesting that the residual Si–Cl sites, with a molecular dipole in the positive direction (Figure 1b), and greater θ_{TFPA} contributed to the positive shift in the band-edge positions. Despite higher S observed for Si(111)–TFPA samples (Figure 3), Si(111)–TFPA samples showed larger shifts in E_{oc} than those observed for Si(111)–MMTFPA samples. This behavior indicated that the overall greater θ_{TFPA} observed for Si(111)–TFPA samples, and inclusion of Si(111)–Cl sites, contributed more to the overall E_{oc} than the high S measured for Si(111)–TFPA samples. The observation of different E_{oc} values for n-Si(111)–MMTFPA and n-Si(111)–TFPA samples in contact with different redox species

indicates that the Fermi level of the semiconductor is not fully pinned by surface states, evidenced by the high observed *S*. The observed decrease in the magnitude of Φ_b for n-Si(111)–TFPA and n-Si(111)–MMTFPA samples was indicative of a substantial positive shift in the band-edge positions of these surfaces relative to Si(111)–CH_3 samples. The E_{oc} observed for n-Si(111)–MMTFPA samples in contact with $Cp^*_2Fe^{+/0}$ and $MV^{2+/+\bullet}$ was further shifted positively by the high *S* observed for samples with high θ_{TFPA}.

The p-Si(111)–MMTFPA and p-Si(111)–TFPA samples exhibited a maximum shift in E_{oc} of +0.10 V relative to p-Si(111)–CH_3 samples in contact with $Cp^*_2Fe^{+/0}$ and $MV^{2+/+\bullet}$. The increase in Φ_b observed for p-Si(111)–MMTFPA samples relative to p-Si(111)–CH_3 samples was approximately 0.5 V, which should produce a larger increase in E_{oc} than was observed. The E_{oc} observed for p-Si(111)–MMTFPA samples in contact with $Cp^*_2Fe^{+/0}$ and $MV^{2+/+\bullet}$ was shifted negatively by the high *S* observed for samples with high θ_{TFPA}. For p-Si samples, the effect on E_{oc} of high *S* opposes the effect on E_{oc} produced by the surface dipole, so the reduced positive shift in E_{oc} achieved for p-Si samples as compared with n-Si samples is consistent with the presence of significant surface recombination at such interfaces.

Monolayer chemistry on Si(111) surfaces can effectively control the interfacial energetics at Si(111) interfaces. Moreover, alkyl monolayers can be applied to a broad range of crystalline, polycrystalline, and thin-film semiconductors without requiring expensive, specialized processing equipment. The electrochemical measurements presented in this work demonstrate that mixed monolayers on Si(111) can produce measurable shifts in the band-edge positions to yield junctions with tunable energetics. The development of methods to reduce *S* while maintaining a surface composition comparable to that of the MMTFPA monolayers presented in this work may enable the use of a broad range of materials in semiconductor devices.

V. CONCLUSIONS

The electrochemical behavior of n- and p-Si(111)–MMTFPA samples in contact with Hg showed that addition of TFPA to the monolayer produced shifts in the band-edge positions, relative to Si(111)–CH_3 surfaces, by ≥0.6 V for n-Si and ≥0.5 V for p-Si samples. Photoelectrochemical measurements in contact with CH_3CN-$Cp^*_2Fe^{+/0}$ and CH_3CN-$MV^{2+/+\bullet}$ demonstrated that the composition of the organic monolayer on the surface yielded shifts in E_{oc} consistent with a net positive molecular dipole at the Si surface. The n-Si(111)–MMTFPA samples exhibited E_{oc} values that shifted by as much as +0.27 V compared with n-Si(111)–CH_3 surfaces, and the p-Si(111)–MMTFPA samples showed E_{oc} values that shifted by up to +0.10 V with respect to the p-Si(111)–CH_3 surface. The change in E_{oc} was limited by surface recombination, suggesting that larger changes in E_{oc} could be achieved by maintaining low S while allowing for comparable levels of F coverage on the surface. Si(111)–MMTFPA surfaces provide a versatile and scalable means of tuning the Si band-edge positions, especially for samples with low θ_{TFPA}. Semiconductor surface chemistry therefore holds promise to allow for control of the interface between semiconductors and functional components, such as metals, metal oxides, catalysts, and conductive polymers.

ACKNOWLEDGEMENTS

We acknowledge the National Science Foundation Grant No. CHE-1214152 for support of supplies and equipment for this work. Instrumentation support was provided by the Molecular Materials Research Center of the Beckman Institute at the California Institute of Technology. N.T.P. acknowledges support from a National Science Foundation Graduate Research Fellowship. B.S.B. and N.T.P. acknowledge support from the National Science Foundation CCI Solar Fuels Program under Grant No. CHE-1305124. N.S.L. acknowledges support from a

National Science Foundation Grant No. CHE-1214152. We thank Dr. Adam C. Nielander, Mr. Christopher W. Roske, and Dr. Kimberly M. Papadantonakis for helpful discussions.

ASSOCIATED CONTENT

Supporting Information

XPS data fitting and quantification, calculation of S, analysis of J-V, J-E, C_{diff}-V, and C_{diff}-E data, discussion of the surface recombination velocity, and supporting Figures S1, S2, and S3. The Supporting Information is made available free of charge on the ACS publications website at DOI:

AUTHOR INFORMATION

Corresponding Author

*E-mail: nslewis@caltech.edu. Telephone: (626) 395-6335.

Notes

The authors declare no competing financial interest.

REFERENCES

1. Walter, M. G.; Warren, E. L.; McKone, J. R.; Boettcher, S. W.; Mi, Q.; Santori, E. A.; Lewis, N. S. Solar Water Splitting Cells. *Chem. Rev.* **2010**, *110*, 6446-6473.

2. Huang, Z.; McKone, J. R.; Xiang, C.; Grimm, R. L.; Warren, E. L.; Spurgeon, J. M.; Lewerenz, H.-J.; Brunschwig, B. S.; Lewis, N. S. Comparison between the Measured and Modeled Hydrogen-Evolution Activity of Ni- or Pt-Coated Silicon Photocathodes. *Int. J. Hydrogen Energy* **2014**, *39*, 16220-16226.

3. McKone, J. R.; Warren, E. L.; Bierman, M. J.; Boettcher, S. W.; Brunschwig, B. S.; Lewis, N. S.; Gray, H. B. Evaluation of Pt, Ni, and Ni-Mo Electrocatalysts for Hydrogen Evolution on Crystalline Si Electrodes. *Energy Environ. Sci.* **2011**, *4*, 3573-3583.

4. Sun, K.; Saadi, F. H.; Lichterman, M. F.; Hale, W. G.; Wang, H.-P.; Zhou, X.; Plymale, N. T.; Omelchenko, S. T.; He, J.-H.; Papadantonakis, K. M., et al. Stable Solar-Driven Oxidation of Water by Semiconducting Photoanodes Protected by Transparent Catalytic Nickel Oxide Films. *Proc. Natl. Acad. Sci. U.S.A.* **2015**, *112*, 3612-3617.

5. Sun, K.; McDowell, M. T.; Nielander, A. C.; Hu, S.; Shaner, M. R.; Yang, F.; Brunschwig, B. S.; Lewis, N. S. Stable Solar-Driven Water Oxidation to O_2(g) by Ni-Oxide-Coated Silicon Photoanodes. *J. Phys. Chem. Lett.* **2015**, *6*, 592-598.

6. Hu, S.; Shaner, M. R.; Beardslee, J. A.; Lichterman, M.; Brunschwig, B. S.; Lewis, N. S., Amorphous TiO_2 Coatings Stabilize Si, GaAs, and GaP Photoanodes for Efficient Water Oxidation. *Science* **2014**, *344*, 1005-1009.

7. O'Leary, L. E.; Strandwitz, N. C.; Roske, C. W.; Pyo, S.; Brunschwig, B. S.; Lewis, N. S. Use of Mixed CH_3–/$HC(O)CH_2CH_2$–Si(111) Functionality to Control Interfacial Chemical and

Electronic Properties During the Atomic-Layer Deposition of Ultrathin Oxides on Si(111). *J. Phys. Chem. Lett.* **2015**, *6*, 722-726.

8. Kim, H. J.; Kearney, K. L.; Le, L. H.; Pekarek, R. T.; Rose, M. J. Platinum-Enhanced Electron Transfer and Surface Passivation through Ultrathin Film Aluminum Oxide (Al_2O_3) on Si(111)–CH_3 Photoelectrodes. *ACS Appl. Mater. Inter.* **2015**, *7*, 8572-8584.

9. Roske, C. W.; Popczun, E. J.; Seger, B.; Read, C. G.; Pedersen, T.; Hansen, O.; Vesborg, P. C. K.; Brunschwig, B. S.; Schaak, R. E.; Chorkendorff, I., et al. Comparison of the Performance of CoP-Coated and Pt-Coated Radial Junction n^+p-Silicon Microwire-Array Photocathodes for the Sunlight-Driven Reduction of Water to H_2(g). *J. Phys. Chem. Lett.* **2015**, *6*, 1679-1683.

10. Warren, E. L.; McKone, J. R.; Atwater, H. A.; Gray, H. B.; Lewis, N. S. Hydrogen-Evolution Characteristics of Ni-Mo-Coated, Radial Junction, n^+p-Silicon Microwire Array Photocathodes. *Energy Environ. Sci.* **2012**, *5*, 9653-9661.

11. Juang, A.; Scherman, O. A.; Grubbs, R. H.; Lewis, N. S. Formation of Covalently Attached Polymer Overlayers on Si(111) Surfaces Using Ring-Opening Metathesis Polymerization Methods. *Langmuir* **2001**, *17*, 1321-1323.

12. Sailor, M. J.; Klavetter, F. L.; Grubbs, R. H.; Lewis, N. S. Electronic Properties of Junctions between Silicon and Organic Conducting Polymers. *Nature* **1990**, *346*, 155-157.

13. Giesbrecht, P. K.; Bruce, J. P.; Freund, M. S. Electric and Photoelectric Properties of 3,4–Ethylenedioxythiophene-Functionalized n-Si/PEDOT:PSS Junctions. *ChemSusChem* **2016**, *9*, 109-117.

14. Bruce, J. P.; Oliver, D. R.; Lewis, N. S.; Freund, M. S. Electrical Characteristics of the Junction between PEDOT:PSS and Thiophene-Functionalized Silicon Microwires. *ACS Appl. Mater. Inter.* **2015**, *7*, 27160-27166.

15. Warren, E. L.; Boettcher, S. W.; Walter, M. G.; Atwater, H. A.; Lewis, N. S. pH-Independent, 520 mV Open-Circuit Voltages of Si/Methyl Viologen$^{2+/+}$ Contacts through Use of Radial n^+p-Si Junction Microwire Array Photoelectrodes. *J. Phys. Chem. C* **2011**, *115*, 594-598.

16. Johansson, E.; Boettcher, S. W.; O'Leary, L. E.; Poletayev, A. D.; Maldonado, S.; Brunschwig, B. S.; Lewis, N. S. Control of the pH-Dependence of the Band Edges of Si(111) Surfaces Using Mixed Methyl/Allyl Monolayers. *J. Phys. Chem. C* **2011**, *115*, 8594-8601.

17. Boettcher, S. W.; Warren, E. L.; Putnam, M. C.; Santori, E. A.; Turner-Evans, D.; Kelzenberg, M. D.; Walter, M. G.; McKone, J. R.; Brunschwig, B. S.; Atwater, H. A., et al. Photoelectrochemical Hydrogen Evolution Using Si Microwire Arrays. *J. Am. Chem. Soc.* **2011**, *133*, 1216-1219.

18. Heller, A. In *Photoeffects at Semiconductor-Electrolyte Interfaces*, American Chemical Society: 1981; Vol. 146, pp 57-77.

19. Zhou, X., Liu, R.; Sun, K.; Friedrich, D.; McDowell, M. T.; Yang, F.; Omelchenko, S. T.; Saadi, F. H.; Nielander, A. C.; Yalamanchili, S., et al. Interface Engineering of the Photoelectrochemical Performance of Ni-Oxide-Coated n-Si Photoanodes by Atomic-Layer Deposition of Ultrathin Films of Cobalt Oxide. *Energy Environ. Sci.* **2015**, *8*, 2644-2649.

20. Smith, W. A.; Sharp, I. D.; Strandwitz, N. C.; Bisquert, J. Interfacial Band-Edge Energetics for Solar Fuels Production. *Energy Environ. Sci.* **2015**, *8*, 2851-2862.

21. Kocha, S. S.; Turner, J. A. Displacement of the Bandedges of $GaInP_2$ in Aqueous Electrolytes Induced by Surface Modification. *J. Electrochem. Soc.* **1995**, *142*, 2625-2630.

22. Hilal, H. S.; Turner, J. A. Controlling Charge-Transfer Processes at Semiconductor/Liquid Junctions. *Electrochim. Acta* **2006**, *51*, 6487-6497.

23. MacLeod, B. A.; Steirer, K. X.; Young, J. L.; Koldemir, U.; Sellinger, A.; Turner, J. A.; Deutsch, T. G.; Olson, D. C. Phosphonic Acid Modification of $GaInP_2$ Photocathodes toward Unbiased Photoelectrochemical Water Splitting. *ACS Appl. Mater. Inter.* **2015**, *7*, 11346-11350.

24. Kim, H. J.; Seo, J.; Rose, M. J. H_2 Photogeneration Using a Phosphonate-Anchored Ni-PNP Catalyst on a Band-Edge-Modified p-Si(111)|Azo Construct. *ACS Appl. Mater. Inter.* **2016**, *8*, 1061-1066.

25. Seo, J.; Kim, H. J.; Pekarek, R. T.; Rose, M. J. Hybrid Organic/Inorganic Band-Edge Modulation of p-Si(111) Photoelectrodes: Effects of R, Metal Oxide, and Pt on H_2 Generation. *J. Am. Chem. Soc.* **2015**, *137*, 3173-3176.

26. Ciampi, S.; Harper, J. B.; Gooding, J. J. Wet Chemical Routes to the Assembly of Organic Monolayers on Silicon Surfaces Via the Formation of Si-C Bonds: Surface Preparation, Passivation and Functionalization. *Chem. Soc. Rev.* **2010**, *39*, 2158-2183.

27. Ciampi, S.; Luais, E.; James, M.; Choudhury, M. H.; Darwish, N. A.; Gooding, J. J. The Rapid Formation of Functional Monolayers on Silicon under Mild Conditions. *Phys. Chem. Chem. Phys.* **2014**, *16*, 8003-8011.

28. Bansal, A.; Li, X.; Lauermann, I.; Lewis, N. S.; Yi, S. I.; Weinberg, W. H. Alkylation of Si Surfaces Using a Two-Step Halogenation/Grignard Route. *J. Am. Chem. Soc.* **1996**, *118*, 7225-7226.

29. Linford, M. R.; Chidsey, C. E. D. Alkyl Monolayers Covalently Bonded to Silicon Surfaces. *J. Am. Chem. Soc.* **1993**, *115*, 12631-12632.

30. Buriak, J. M. Illuminating Silicon Surface Hydrosilylation: An Unexpected Plurality of Mechanisms. *Chem. Mater.* **2014**, *26*, 763-772.

31. Buriak, J. M.; Sikder, M. D. H. From Molecules to Surfaces: Radical-Based Mechanisms of Si–S and Si–Se Bond Formation on Silicon. *J. Am. Chem. Soc.* **2015**, *137*, 9730-9738.

32. Royea, W. J.; Juang, A.; Lewis, N. S. Preparation of Air-Stable, Low Recombination Velocity Si(111) Surfaces through Alkyl Termination. *Appl. Phys. Lett.* **2000**, *77*, 1988-1990.

33. Plymale, N. T.; Kim, Y.-G.; Soriaga, M. P.; Brunschwig, B. S.; Lewis, N. S. Synthesis, Characterization, and Reactivity of Ethynyl- and Propynyl-Terminated Si(111) Surfaces. *J. Phys. Chem. C* **2015**, *119*, 19847-19862.

34. O'Leary, L. E.; Johansson, E.; Brunschwig, B. S.; Lewis, N. S. Synthesis and Characterization of Mixed Methyl/Allyl Monolayers on Si(111). *J. Phys. Chem. B* **2010**, *114*, 14298-14302.

35. Webb, L. J.; Lewis, N. S. Comparison of the Electrical Properties and Chemical Stability of Crystalline Silicon(111) Surfaces Alkylated Using Grignard Reagents or Olefins with Lewis Acid Catalysts. *J. Phys. Chem. B* **2003**, *107*, 5404-5412.

36. Webb, L. J.; Michalak, D. J.; Biteen, J. S.; Brunschwig, B. S.; Chan, A. S. Y.; Knapp, D. W.; Meyer, H. M.; Nemanick, E. J.; Traub, M. C.; Lewis, N. S. High-Resolution Soft X-Ray Photoelectron Spectroscopic Studies and Scanning Auger Microscopy Studies of the Air Oxidation of Alkylated Silicon(111) Surfaces. *J. Phys. Chem. B* **2006**, *110*, 23450-23459.

37. Bansal, A.; Lewis, N. S. Stabilization of Si Photoanodes in Aqueous Electrolytes through Surface Alkylation. *J. Phys. Chem. B* **1998**, *102*, 4058-4060.

38. Maldonado, S.; Knapp, D.; Lewis, N. S. Near-Ideal Photodiodes from Sintered Gold Nanoparticle Films on Methyl-Terminated Si(111) Surfaces. *J. Am. Chem. Soc.* **2008**, *130*, 3300-3301.

39. Maldonado, S.; Lewis, N. S. Behavior of Electrodeposited Cd and Pb Schottky Junctions on CH_3-Terminated n-Si(111) Surfaces. *J. Electrochem. Soc.* **2009**, *156*, H123-H128.

40. Maldonado, S.; Plass, K. E.; Knapp, D.; Lewis, N. S. Electrical Properties of Junctions between Hg and Si(111) Surfaces Functionalized with Short-Chain Alkyls. *J. Phys. Chem. C* **2007**, *111*, 17690-17699.

41. Hunger, R.; Fritsche, R.; Jaeckel, B.; Jaegermann, W.; Webb, L. J.; Lewis, N. S. Chemical and Electronic Characterization of Methyl-Terminated Si(111) Surfaces by High-Resolution Synchrotron Photoelectron Spectroscopy. *Phys. Rev. B* **2005**, *72*, 045317.

42. Wong, K. T.; Lewis, N. S. What a Difference a Bond Makes: The Structural, Chemical, and Physical Properties of Methyl-Terminated Si(111) Surfaces. *Acc. Chem. Res.* **2014**, *47*, 3037-3044.

43. O'Leary, L. E.; Rose, M. J.; Ding, T. X.; Johansson, E.; Brunschwig, B. S.; Lewis, N. S. Heck Coupling of Olefins to Mixed Methyl/Thienyl Monolayers on Si(111) Surfaces. *J. Am. Chem. Soc.* **2013**, *135*, 10081-10090.

44. Lattimer, J. R. C.; Blakemore, J. D.; Sattler, W.; Gul, S.; Chatterjee, R.; Yachandra, V. K.; Yano, J.; Brunschwig, B. S.; Lewis, N. S.; Gray, H. B. Assembly, Characterization, and Electrochemical Properties of Immobilized Metal Bipyridyl Complexes on Silicon(111) Surfaces. *Dalton Trans.* **2014**, *43*, 15004-15012.

45. Lattimer, J. R. C.; Brunschwig, B. S.; Lewis, N. S.; Gray, H. B. Redox Properties of Mixed Methyl/Vinylferrocenyl Monolayers on Si(111) Surfaces. *J. Phys. Chem. C* **2013**, *117*, 27012-27022.

46. Rivillon, S.; Chabal, Y. J.; Webb, L. J.; Michalak, D. J.; Lewis, N. S.; Halls, M. D.; Raghavachari, K. Chlorination of Hydrogen-Terminated Silicon (111) Surfaces. *J. Vac. Sci. Technol. A* **2005**, *23*, 1100-1106.

47. Grimm, R. L.; Bierman, M. J.; O'Leary, L. E.; Strandwitz, N. C.; Brunschwig, B. S.; Lewis, N. S. Comparison of the Photoelectrochemical Behavior of H-Terminated and Methyl-Terminated Si(111) Surfaces in Contact with a Series of One-Electron, Outer-Sphere Redox Couples in CH_3CN. *J. Phys. Chem. C* **2012**, *116*, 23569-23576.

48. Hendrickson, D. N.; Sohn, Y. S.; Gray, H. B. Magnetic Susceptibility Study of Various Ferricenium and Iron(III) Dicarbollide Compounds. *Inorg. Chem.* **1971**, *10*, 1559-1563.

49. Megehee, E. G.; Johnson, C. E.; Eisenberg, R. Optical Versus Thermal Electron Transfer between Iridium(I) Maleonitriledithiolate Complexes and Methyl Viologen. *Inorg. Chem.* **1989**, *28*, 2423-2431.

50. Webb, L. J.; Rivillon, S.; Michalak, D. J.; Chabal, Y. J.; Lewis, N. S. Transmission Infrared Spectroscopy of Methyl- and Ethyl-Terminated Silicon(111) Surfaces. *J. Phys. Chem. B* **2006**, *110*, 7349-7356.

51. Li, Y.; O'Leary, L. E.; Lewis, N. S.; Galli, G. Combined Theoretical and Experimental Study of Band-Edge Control of Si through Surface Functionalization. *J. Phys. Chem. C* **2013**, *117*, 5188-5194.

52. Kratochvil, B.; Lorah, E.; Garber, C. Silver-Silver Nitrate Couple as Reference Electrode in Acetonitrile. *Anal. Chem.* **1969**, *41*, 1793-1796.

53. Kim, N. Y.; Laibinis, P. E. Derivatization of Porous Silicon by Grignard Reagents at Room Temperature. *J. Am. Chem. Soc.* **1998**, *120*, 4516-4517.

54. Socrates, G. *Infrared and Raman Characteristic Group Frequencies: Tables and Charts*, 3rd ed.; John Wiley & Sons Ltd.: Chichester, West Sussex, England, 2001.

55. Larkin, P. J. *Ir and Raman Spectroscopy: Principles and Spectral Interpretation*; Elsevier: Waltham, MA, USA, 2011.

56. Stuart, B. H. *Infrared Spectroscopy: Fundamentals and Applications*; John Wiley & Sons Ltd.: Chichester, West Sussex, England, 2004.

57. Jaeckel, B.; Hunger, R.; Webb, L. J.; Jaegermann, W.; Lewis, N. S. High-Resolution Synchrotron Photoemission Studies of the Electronic Structure and Thermal Stability of CH_3- and C_2H_5-Functionalized Si(111) Surfaces. *J. Phys. Chem. C* **2007**, *111*, 18204-18213.

58. Moulder, J. F.; Stickle, W. F.; Sobol, P. E.; Bomen, K. D. *Handbook of X-Ray Photoelectron Spectroscopy: A Reference Book of Standard Spectra for Identification and Interpretation of XPS Data*; Physical Electronics USA, Inc.: Chanhassen, Minnesota, 1995.

59. Collins, G.; O'Dwyer, C.; Morris, M.; Holmes, J. D. Palladium-Catalyzed Coupling Reactions for the Functionalization of Si Surfaces: Superior Stability of Alkenyl Monolayers. *Langmuir* **2013**, *29*, 11950-11958.

60. *Handbook of Chemistry and Physics*, 75th ed.; CRC Press, Inc. : Boca Raton, Florida, 1994.

61. Trasatti, S. The Absolute Electrode Potential: An Explanatory Note. *Pure Appl. Chem.* **1986**, *58*, 955-966.

62. Dekker, M. *Standard Potentials in Aqueous Solution*; CRC Press, Inc.: New York, 1985.

63. Bird, C. L.; Kuhn, A. T. Electrochemistry of the Viologens. *Chem. Soc. Rev.* **1981**, *10*, 49-82.

TOC Graphic